

# Supernova Enrichment of Dwarf Spheroidal Galaxies

P. Chris Fragile, Stephen D. Murray, Peter Anninos

*University of California, Lawrence Livermore National Laboratory, P.O. Box 808, Livermore, CA 94550*

and

Douglas N. C. Lin

*University of California, Lick Observatory, Santa Cruz, CA 95064*

## ABSTRACT

Many dwarf galaxies exhibit sub-Solar metallicities, with some star-to-star variation, despite often containing multiple generations of stars. The total metal content in these systems is much less than expected from the heavy element production of massive stars in each episode of star formation. Such a deficiency implies that a substantial fraction of the enriched material has been lost from these small galaxies. Mass ejection from dwarf galaxies may have important consequences for the evolution of the intergalactic medium and for the evolution of massive galaxies, which themselves may have formed via the merger of smaller systems. We report here the results of three-dimensional simulations of the evolution of supernova-enriched gas within dwarf spheroidal galaxies (dSph's), with the aim of determining the retention efficiency of supernova ejecta. We consider two galaxy models, selected to represent opposite ends of the dSph sequence. One contains  $10^6 M_{\odot}$  of gas, and the other  $5.5 \times 10^6 M_{\odot}$ . In both, the baryonic-to-dark matter ratio is assumed to be 0.1. The total binding energies of the gas in the two models are  $9.8 \times 10^{50}$  erg and  $1.6 \times 10^{52}$  erg. For each model galaxy we investigate a number of scenarios. The simplest is a single supernova within a smooth gas distribution. We also investigate the evolution of ten supernovae, within initially smooth gas distributions, occurring over time spans of either 10 or 100 Myr. Finally, we investigate the effects of ten supernovae occurring over 10 Myr in a medium filled with hot “bubbles,” such as would be expected in the presence of an initial generation of hot stars. For models with only a single supernova, no enriched material is lost from the galaxies. When multiple supernovae occur within an initially smooth gas distributions, less than half of the enriched gas is lost from the galaxy (fractional losses range from 0-47%). Most of the enriched gas is lost, however, from the cores of the galaxies. In the presence of an initially disturbed gas distribution, 6% or less of the enriched gas remains in the core, and much is lost from the galaxies as a whole (47% and 71% for the larger and smaller galaxy models, respectively). If subsequent star formation occurs predominantly within the core where most of the residual gas is concentrated, then these results could explain the poor self-enrichment efficiency observed in dwarf galaxies.

*Subject headings:* galaxies: dwarf — galaxies: evolution — hydrodynamics — methods: numerical — supernovae: general

## 1. Introduction

In cosmological models dominated by cold dark matter (CDM), the amplitude of fluctuations increases toward shorter wavelengths. Small galaxies are therefore likely to be the first to form, and large galaxies

subsequently form through the merger of smaller systems (e.g. White & Rees 1978; Blumenthal et al. 1984; Cole et al. 1994; Klypin, Nolthenius, & Primack 1997; Navarro, Frenk & White 1997). Small systems observed today, such as dwarf spheroidal galaxies (dSph’s), may thus represent surviving “building blocks” of larger galaxies, and therefore much attention has been paid to understanding the gas evolution and first generation of star formation within them (e.g. Lin & Murray 1994; Navarro & White 1994; Mori et al. 1997; Weil, Eke & Efstathiou 1998; Klypin et al. 1999; Sommer-Larsen, Gelato & Vedel 1999; Burkert 2000; Mori & Burkert 2000; Dong, Murray, & Lin 2003).

Their small sizes might indicate that dSph’s can also serve as relatively simple laboratories to study the effects of various physical processes upon star formation. In spite of their dynamical simplicity, however, they are found to have a wide range of star-formation and enrichment histories, with few clear trends (Mateo 1998; Grebel 2001; Harbeck et al. 2001). The data therefore indicate that multiple factors have affected star formation in dSph’s, making them important and interesting objects for the study of early star formation in galaxies. Factors that may have influenced star formation in dSph’s include their exposure to external ultraviolet radiation, the depth of their gravitational potential, their overall mass, their interactions with other dwarf systems, and their proximity to neighboring massive systems. The work described here is part of a series of papers in which we examine these various physical factors, with the goal of determining their relative importance upon the evolution of the dwarf galaxies.

An important observational fact concerning dSph’s is that almost all have multiple generations of stars, with many showing clear evidence of having undergone bursts of star formation, generally with one dominant, and multiple weaker events (Mateo 1998; Grebel 2001). In some systems, multiple generations of star formation may also be inferred from the observed spread in the metallicity of individual stars within them (Lehnert et al. 1992; Suntzeff et al. 1993; Côté, Oke, & Cohen 2000; Shetrone, Côté, & Sargent 2001). Multiple generations of stars are also inferred from Hubble Space Telescope observations of stellar populations in dwarf systems that are resolved both spatially as well as temporally (Gallagher et al. 1998; Dohm-Palmer et al. 1998a,b, 2002). Most systems with multiple generations of stars, however, display less self-enrichment than would be expected from their star-formation histories, and the total mass of heavy elements contained within these galaxies is far less than that expected to be produced by the massive stars that would have formed along with the currently observed low-mass stellar population (Smecker-Hane et al. 1996; Grebel 1997).

Star formation within dSph’s may be strongly inhibited at early times by the ultraviolet background radiation (Efstathiou 1992; Quinn, Katz, & Efstathiou 1996; Kepner, Babul, & Spergel 1997; Navarro & Steinmetz 1997; Weinberg, Hernquist & Katz 1997; Barkana & Loeb 1999; Benson et al. 2002). External triggers may still, however, lead to cooling and star formation (Lin & Murray 1994; Dong, Murray, & Lin 2003). Following an initial burst of star formation, the remaining gas within the galaxy may be heavily affected by photionization, stellar winds, and supernova explosions. Such stellar feedback has been studied extensively as a means of driving the evolution of stellar systems. Photoionization feedback has been proposed as a means by which star formation may be self-regulated in dwarf systems (Babul & Rees 1992; Andersen & Burkert 2000; Dong, Murray, & Lin 2003). In systems the size of globular clusters, photoionization-driven winds may lead to extensive mass loss, sufficient even to completely terminate star formation (Peebles & Dicke 1968; Tenorio-Tagle et al. 1986). In small galactic systems as extended as dSph’s, however, it is ineffective at driving mass loss (Noriega-Crespo et al. 1989).

Energy input from the multiple supernova events following a burst of star formation may also be a means of driving mass loss. Substantial mass loss has been found in simulations of low-mass disk systems subjected to multiple supernovae (Mac Low & Ferrara 1999). Mass loss is expected to be less efficient, however, from

more rounded systems, in which heated gas must travel a greater distance through the ambient medium before it is able to leave the system. Studies of the evolution of supernovae in high redshift dwarf systems find that the high densities and resultant high cooling efficiencies and external pressures make it relatively easy for dwarf galaxies to retain mass following supernova explosions. In order for them to experience significant mass loss, high ( $\gtrsim 10\%$ ) star formation efficiencies are required (Dekel & Silk 1986; Mac Low & McCray 1988; Madau, Ferrara, & Rees 2001; Mori, Ferrara, & Madau 2002). Even at later times, high star formation efficiencies may be required in order for supernovae to drive extensive mass loss, due to radiative losses (Larson 1974). We note, however, that mass loss through the Lagrange points may also lead to significant rates of mass loss, if the gas within the galaxy is ionized either by external or internal sources (Murray, Dong & Lin 2003). Extensive star formation is, therefore, not required in order to account for the total removal of gas from dSph's, as observed today.

The presence of multiple generations of stars within dSph's implies that their early star formation efficiencies were not so high as to lead to extensive mass loss. The poor self-enrichment of later generations, however, suggests that enriched material from supernovae was preferentially lost, leaving behind gas that was at most slightly enriched. It was from this poorly enriched gas that subsequent generations of stars then formed. It is therefore of interest to examine the evolution of enriched material within dwarf galaxies that have undergone relatively inefficient bursts of star formation. In this paper, we examine the loss of enriched material from dSph's which are subjected to a number of supernova events. We proceed in § 2 by describing the numerical method and the setup of the models. The results of the simulations are described in § 3 and § 4. The possible consequences for the evolution of dwarf galaxies are discussed in § 5.

## 2. Numerical Method

### 2.1. The Numerical Code

The models discussed below have been computed using Cosmos, a massively parallel, multidimensional, radiation-chemo-hydrodynamics code for both Newtonian and relativistic flows developed at Lawrence Livermore National Laboratory. The relativistic capabilities and tests of Cosmos are discussed in Anninos & Fragile (2003). Tests of the Newtonian hydrodynamics options and of the internal physics relevant to the current work are presented in Anninos, Fragile & Murray (2002), and so we shall not discuss those in detail here.

Because we shall be examining the effects of having multiple supernova explosions at random locations throughout the cores of dwarf galaxies, we cannot make any assumptions regarding the symmetry of the systems. As a consequence, our models are run in three-dimensions on a Cartesian mesh. Most of the simulations are run with resolutions of  $128^3$  zones.

### 2.2. Radiative Cooling

Chemistry is not followed in these simulations. Instead, local cooling is given by the following cooling function, based in part on an equilibrium (hydrogen recombination and collisional excitation) cooling curve

$$\Lambda(T, \rho) = \left[ \sum_i \dot{\epsilon}_i(T)(f_I \rho)^2 + \dot{\epsilon}_M(T)(f_M \rho)^2 \right] \times \begin{cases} e^{(T-T_{min})/\delta T} & \text{if } T \leq T_{min}, \\ 1 & \text{otherwise,} \end{cases} \quad (2-1)$$

where  $\dot{e}_M$  is the temperature-dependent cooling rate from metals (including carbon, oxygen, neon, and iron lines, assuming a metallicity  $Z = 0.03Z_\odot$ ),  $\dot{e}_i$  is the cooling rate from hydrogen and helium lines,  $f_M$  is the mass fraction of metals taken to be  $6 \times 10^{-4}$ ,  $f_I$  is an estimate of the ionization fraction, defined as  $\min(1, \max(0, (T_{eV} - T_c)/3))$  with  $T_c = 1eV$  to match roughly the upper and lower bounds in the equilibrium model described in Anninos, Fragile & Murray (2002),  $T = (\Gamma - 1)e\mu m_p / (k_B\rho(1 + f_I))$  is the gas temperature in Kelvin,  $\rho$  is the gas density,  $e$  is the internal energy density of the gas,  $\mu$  is the mean molecular weight, taken to be unity,  $m_p$  is the proton mass, and  $k_B$  is Boltzmann’s constant. The exponential is introduced to suppress cooling at low temperature (here  $T_{min} = 10^4$  K, with width  $\delta T = 500$  K). The initial temperature of the gas in the systems considered here is 8200 K, representing a state which is partially ionized by the background. The rapid decrease of cooling below  $10^4$  K simulates the effects of heat sources and the exponential decay of electron density below about 1 eV in equilibrium models. This prevents the gas from radiatively cooling significantly below its initial temperature.

Our choice of metallicity is motivated by the fact that we are examining the evolution of young dSph’s, which have not had a chance to undergo significant self-enrichment. The value  $Z = 0.03Z_\odot$ , is appropriate to the older generations of stars observed within dSph’s (Grebel 2001).

### 2.3. Gravity

The galaxies are modeled as non-self gravitating gas within a fixed dark-matter potential. The omission of self-gravity is reasonable, given that the gravitational potential of dwarf galaxies with  $M_g \lesssim 10^9 M_\odot$  is dominated by the dark-matter halo (Persic, Salucci, & Stel 1996), where  $M_g$  is the mass of the visible (gas plus stellar) matter. The shape of the potential is given by a modified Hubble profile (Binney & Tremaine 1987)

$$\phi(r < R_t) = \frac{G\tilde{M}}{R_c} \left\{ 1 - \frac{\ln[x + (1 + x^2)^{1/2}]}{x} \right\}, \quad (2-2)$$

where  $x = r/R_c$ ,  $R_c$  is the core radius, and

$$\tilde{M} = M_d \left\{ \ln[x_t + (1 + x_t^2)^{1/2}] - x_t(1 + x_t^2)^{-1/2} \right\}^{-1}, \quad (2-3)$$

where  $M_d$  is the dark-matter mass,  $x_t = R_t/R_c$ , and  $R_t$  is the tidal radius. This potential has a simple form, while retaining the essential behavior for the shape of potentials which are generally observed in dSph’s (Burkert 1995). The gas is initialized to be isothermal and in hydrostatic equilibrium within the potential, such that the density

$$\rho = \rho_0 e^{-\phi/c_s^2}, \quad (2-4)$$

where  $c_s$  is the isothermal sound speed. The value of  $\rho_0$  is scaled to give the desired gas mass  $M_g$  within  $R_t$ . The effects of a tidal radius are included by flattening the potential beyond  $R_t$ . Beyond  $R_t$ , the gas density is also decreased by a factor of 0.01, and the temperature is correspondingly increased in order to maintain hydrostatic equilibrium. This simplified treatment of the galaxy’s surroundings allows us to focus on the physics within the dwarf galaxy itself.

### 2.4. Boundary Conditions

To minimize the effects of the computational boundaries on the galaxy evolution, we choose the size of the grid,  $l$ , such that  $2R_t = 0.8l$ . Our boundary zones remain static throughout these simulations,

maintaining their initial density and temperature. This choice of boundary conditions resulted in fewer disruptive reflections than flat (vanishing first derivative) boundaries and less spurious mass loss than outflow boundaries. We have verified that, in the absence of supernovae, the models remain static for several dynamical times.

## 2.5. Galaxy Parameters

Two different model galaxies have been examined. Their parameters are given in Table 1, which lists the dark-matter mass  $M_d$ , gas mass  $M_g$ , core radius  $R_c$ , the central gas density  $\rho_0$ , the dynamical time of the galaxy  $\tau_d$  (defined below), the total gravitational binding energy of the gas,  $\Phi$ , and the total thermal energy of the gas,  $E_{th}$ , for each model. The parameters of galaxies 1 and 2 are chosen to be close to those of Leo II and Fornax, respectively, objects near the ends of the distribution for dSph’s (Mateo 1998). For both model galaxies, the ratio of the tidal to the core radii is chosen to be  $R_t/R_c = 3$ . We note that the central densities of the two models are similar, in spite of their having different masses, due to the larger core radius of Model 2. In Figure 1, we plot the square root of the absolute value of the normalized gravitational potential ( $|\phi - \phi_t|^{1/2}$ ) as a function of radius for the two galaxy models. This function gives a good estimate of the local escape velocity.

It may also be noted from Table 1 that the total binding energy of the gas in the two models is of the order of the energy input of 1-10 supernovae, which is precisely the range covered in our models (see below). It might therefore be expected that the energy input from supernovae would lead to extensive mass loss from the systems. As shall be seen, however, this is only the case when radiative cooling is neglected. As has been noted in earlier studies (Larson 1974), radiative losses cause the deposition of energy from supernovae to be relatively inefficient. We discuss this point further and examine the effects of radiative losses in § 3.2.

## 2.6. Treatment of Supernovae

In this study, supernovae are simulated by adding  $10^{51}$  erg of internal energy to the gas over finite regions. The internal energy is injected over an approximately spherical volume with a “top-hat” profile of 3-4 zones radius. Computing time constraints limit our resolutions, and we are therefore unable to maintain zoning sufficiently fine as to resolve the supernova shocks and the cooling regions immediately behind them. The results are therefore vulnerable to numerical over-cooling of the shocked gas, which would lead to an underestimate of the effects of the supernovae. This potential problem is exacerbated by having the energy initially deposited into the internal energy of the gas, after which it evolves to a Sedov-Taylor solution. In addition, the artificial viscosity used to capture shocks spreads out shock heating over a few zones. Gas may, therefore, spend multiple timesteps at elevated temperatures, possibly near the peak of the cooling curve. This can cause further over-cooling of the gas, significantly affecting the hydrodynamic evolution. In order to prevent over-cooling of the gas we simultaneously employ two techniques. First, we do not allow cooling within a supernova until it has roughly doubled in radius. Second, we follow the common procedure of preventing cooling of the gas during shock passage (Shapiro & Struck-Marcell 1985; Blondin, Fryxell, & Konigl 1990; Anninos & Norman 1994). To accomplish this in a three-dimensional problem, where shocks may occur in any direction, a simple scalar criterion is needed. We find, in practice, that the ratio of the artificial viscous heating term to gas pressure is an adequate filter. Thus, cooling is turned off whenever  $Q/P > 0.1$ . The effects of these techniques will be explored in § 3.2.

In order to follow the evolution of the supernova-enriched material, we add a tracer fluid to the zones in which the supernova energy is initially deposited. The tracer is a passive quantity that is advected in the same manner as density.

The simulations discussed below include either one or ten supernovae. In the cases with only a single supernova, it is set off either at the center of the system or at the core radius. In these cases we are able to take advantage of symmetries in the problem to reduce the required computational resources. For a single supernova set off at the center of the galaxy, we employ  $x$ ,  $y$ , and  $z$  symmetries and run a single octant with reflective boundary conditions at the  $x = 0$ ,  $y = 0$ , and  $z = 0$  planes. For a single supernova at  $R_c$ , we can invoke symmetry in two dimensions and run a quadrant with reflective boundaries along two planes. If ten supernovae are included, the first is set off at  $R_c$  at the start of the simulation. The rest are chosen to occur at random orientations to the center of the system. The radii at which they occur are chosen at random, weighted by the enclosed mass of gas, and constrained to be within  $R_c$ . The latter constraint is due to the expectation that bursts of star formation are expected to be located predominantly in galactic cores, where gas densities are highest (Dong, Murray, & Lin 2003). The timescale over which supernovae occur is determined by the timescale of the burst of star formation that led to the formation of the progenitor stars, and by the spread in masses, and therefore lifetimes, of the progenitor stars. To examine the effects of reasonable variations in these factors, the supernovae in the models are set off at times chosen randomly within total spans of either 10 or 100 Myr.

## 2.7. The Form of the Interstellar Medium

In most of our models, the gas density varies smoothly, following Equation 2-4. Following a burst of star formation in a dwarf galaxy, however, such a smooth density distribution is unlikely to actually be found. Instead, ionizing photons and winds from massive stars, and turbulent motions shall all lead to a very irregular gas distribution for the interstellar medium (ISM). The low density regions in such a distribution may enhance the loss of material from supernovae, and so it might be expected that the form of the gas distribution could play a role in the ability of a galaxy to retain enriched gas. In order to explore the role of the gas distribution, two of the models include 100 “bubbles,” each five zones in radius, whose density is decreased by a factor of five relative to the surrounding gas. The physical interpretation of these bubbles is that they are cleared by ionizing photons and winds from massive stars. The temperature within the bubbles is increased, such that they remain in pressure equilibrium with the surrounding gas. The bubbles are selected to have random orientations around the center of the galaxy and they are not, in general, co-located with the supernovae, which is justified by the fact that during their main-sequence life span, massive stars may move up to 100 pc from their initial position. The distances of the bubbles from the galaxy center are selected at random, weighted by enclosed mass and constrained to be no more than  $0.6R_t$  from the center of the galaxy. Once the bubbles are placed, the density of the entire system is increased by a common factor to preserve the original mass of the galaxy. To simulate the presence and evolution of the hot stars causing the bubbles, cooling is not allowed within the bubbles for 0.5 dynamical times after the supernovae end.

In physical units, the bubble radii correspond to approximately 40 pc for Model 1 and 100 pc for Model 2, comparable to the radii of Strömgren spheres. The total filling factor for the bubbles within  $0.6R_t$  is approximately 30%, i.e. the ISM is highly irregular in form. For typical stellar initial mass functions, the number of supernovae and bubbles in our models represent overall star formation efficiencies for the galaxies of less than 1%.

## 2.8. Other Physics

The models discussed below do not include the effects of conduction or of magnetic fields. The effects of thermal conduction may be estimated from the conductive flux

$$F_c = \kappa T^{5/2} \nabla T, \quad (2-5)$$

where  $\kappa = 6 \times 10^{-7} \text{ erg cm}^{-2} \text{ s}^{-1} \text{ K}^{-7/2}$  (Spitzer 1956). The total energy flow across the interface between an expanding bubble of heated gas may be compared with the radiative energy losses from within the volume of the bubble. Radiative losses rapidly lead to a relatively shallow temperature gradient, greatly reducing the conductive flux, with the result that conductive losses are found to be much less important than radiative emission in our models, justifying the omission of conduction.

The presence of even weak magnetic fields would greatly hamper conduction, further reducing its importance (Rosner & Tucker 1989). Stronger magnetic fields could potentially affect the hydrodynamics. A strong, ordered magnetic field would tend to direct the flow of gas to be one-dimensional, whereas a strong field that was tangled on small scales would act as an additional pressure term, possibly helping to contain gas within the galaxies. The magnetic field would be expected to noticeably affect the flow if the magnetic pressure were comparable to the ambient gas pressure, which, for our models, requires  $B \approx 5 \mu\text{G}$ , greater than or comparable to values measured in the local ISM (Heiles 1987). Whether dwarf systems could generate fields with strengths comparable to those in our own Galaxy is uncertain, as are the actual field strengths present today in dwarf galaxies. Magnetic fields therefore remain an uncertain quantity. If present in young dSph's at magnitudes comparable to the local ISM, then their affect would be expected to be comparable to that of the ambient gas pressure, having a quantitative affect upon our results, but not affecting the qualitative conclusion that enriched material can be preferentially lost from dwarf systems.

## 3. Model Results

The parameters of the models that we have computed are shown in Table 2. Listed in the table for each model are the galaxy model used, the number of supernovae included  $N_{SN}$ , the timescale over which the supernovae occur  $\tau_{SN}$ , and the number of bubbles included in the galaxy  $N_{\text{bub}}$ . Variations of many of these base models are also examined (see below). All of the runs are summarized in Table 3, where the variations are indicated by numbers following the letters of the base models. The tabulated results include the percentage of tracer lost from the core as well as that lost beyond  $R_t$ , and also the percentage of gas mass lost from the galaxies. The core tracer loss is measured after at least 2.5 dynamical times for the galaxies, while the tracer and mass losses beyond  $R_t$  are estimated from the global minima (see below). In this section, we discuss the results of the models, and we follow with a discussion of the reasons for the differences among them in § 4.

### 3.1. Single Supernova Events

In Models A1 and B1, single supernovae are set off in the centers of the two model galaxies. For both models, all of the tracer remains within the core of the galaxy. The lack of tracer loss is expected, given the core masses of the low and high mass models, which are approximately  $1.6 \times 10^5$  and  $3 \times 10^6 M_\odot$ , respectively. Such large masses of gas have no trouble containing the ejecta from single supernova events.

We have also run versions of Models A and B, in which a single supernova was triggered at  $R_c$  (Models A2 and B2, respectively). Although this obviously resulted in significant loss of tracer from the core, only the low mass galaxy (Model 1) showed any loss of tracer from the system (30%). We conclude from this that multiple supernovae appear to be required in order for large fractions of enriched material to be lost from within rounded galaxies, even as small as those considered here.

### 3.2. Multiple Supernovae in Undisturbed Systems

#### 3.2.1. Low Mass Galaxy Models

In Models C and D, 10 supernovae are set off at random locations within the core of the initially undisturbed galaxy Model 1. The supernovae are triggered at random times over a span of 10 Myr for Model C and 100 Myr for Model D.

We further utilize Model C to test the effects of resolution upon our results and to explore the impact of different choices for radiative cooling and metallicity. Model C1 is our control model, as it utilizes our standard cooling options, resolution, and metallicity. Hence, this model is most comparable to Models A, B, D, E, F, G, and H. Model C2 utilizes the same cooling options, but has a spatial resolution reduced by a factor of two. Model C3 tests the effect of not shutting off cooling at shock fronts by ignoring the  $Q/P > 0.1$  criterion described in § 2.6. Similarly, Model C4 tests the effect of not shutting off cooling in the initial supernova region by ignoring that requirement. Model C5 ignores both the  $Q/P$  condition and the requirement to shut off cooling in the initial supernova region, and thus represents results with cooling turned on “everywhere,” and so likely suffers from significant over-cooling. Model C6 tests the effect of our choice of metallicity, by using a metallicity  $Z = 0.3Z_\odot$ , an order of magnitude higher than that of Model C1. Finally Model C7 represents the extreme case in which radiative cooling is turned off everywhere, and the gas may cool only by adiabatic expansion. We proceed by first comparing the results of Models C1 and D. The effects of the variations of Model C are discussed in § 3.2.3.

In Figure 2 are shown snapshots of two-dimensional slices of the density evolution through the central galactic plane for Model C1. The snapshots cover a span of approximately 100 Myr. The evolution of one of the tracer fluids from Model C1 is shown in Figure 3, at times corresponding to the frames in Figure 2. This tracer is associated with the initial supernova (triggered at  $R_c$ ), visible in the second frame of Figure 2. Figure 4 shows the time evolution of the amount of tracer contained within  $R_t$  (solid curves) and  $R_c$  (dashed curves) for Models C1 and D. The enriched material from each supernova is labeled with a different tracer, and the evolution is shown individually for each. On the curves, time is presented in code units, where a unit of one represents approximately the dynamical time of the galaxy, defined as

$$\tau_d \equiv \frac{R_t}{c_s}, \quad (3-1)$$

where  $c_s$  is the sound speed of the gas. The time unit for galaxy Model 1 is 48.2 Myr.

Significant ( $\gtrsim 80\%$ ) loss of tracer is seen from within  $R_c$  for both models, although Model C1 loses a greater fraction than does Model D. In Model C1, the loss of tracer is accompanied by an initial loss of approximately 50% of the gas from the core. The core mass returns to its initial value, however, within  $\approx \tau_d$ . This recovery of the initial core mass without an accompanying recovery of tracer implies that the tracer does not mix well with the gas in the core. In Model D, where the supernovae occur over a longer timescale, the evolution of the core mass is much gentler, yet the same conclusion holds.



Additionally, in Model C1, nearly one-half (47%) of the tracer moves beyond  $R_t$ , while almost 20% does so in Model D. This material also does not mix well with the surrounding gas, as shown in Figure 3, where the tracer can be seen to evolve as a nearly cohesive unit. As can be seen in Figure 4 (and subsequent figures), some of the tracer that moves beyond  $R_t$  later returns to the galaxy. This behavior is an artifact of our boundary conditions. At the boundaries, the gas properties are held constant in time, which can artificially prevent material from leaving the grid, and drive it back to the galaxy. In actuality, material that moves beyond the tidal radius is unlikely to return to the dwarf galaxy on the time scales shown here, but shall instead follow a separate orbit around the parent galaxy. The gas which escapes from the galaxy in Model C1 does so with velocities of only 5-7 km s<sup>-1</sup>, much less than the orbital speed of the dSph satellites around the Milky Way. During an orbit, therefore, the gas would not move substantially away from the dSph, and would possibly re-encounter it on the next apogalacticon passage (Dong, Lin, & Oh 2002).

The loss of tracer from the galaxy is accompanied by overall mass loss, as can be seen in Figure 5, which shows the mass contained within  $R_t$  (solid curves) and  $R_c$  (dashed curves) for Models C1 and D. The inflow due to the outer boundary conditions is apparent in both figures. As discussed above, in the absence of a confining external medium, gas is actually unlikely to return to the system after it moves to beyond  $R_t$ . The total mass loss to be expected in the models may therefore be represented by the first minima shown in Figure 5, which represent 36% and 21% for Models C1 and D, respectively.

### 3.2.2. High Mass Galaxy Models

Models E and F were similar to C and D, except that the higher mass galaxy model (Model 2) was used. The evolution of the tracer fluids for these models is shown in Figure 6, displayed as in Figure 4. The time unit for galaxy Model 2 is 130 Myr. A large fraction of the tracer is lost from the core, though less than seen in Models C1 and D, and almost no tracer is lost beyond  $R_t$ . Such differences are expected given the larger mass of this galaxy model. Little mass loss is seen from the system in Models E and F, as expected from the tracer evolution.

### 3.2.3. The Effects of Numerical Techniques

As discussed above, we tested the effects of resolution upon our results by reducing the spatial resolution of Model C2 by a factor of two relative to Model C1. In order to keep other factors as similar as possible, the physical radii over which the supernova energies were added was kept the same, requiring that the energy be added over many fewer zones. The results were similar to Model C1, with almost identical amounts of tracer loss from the core and overall mass loss. Somewhat less tracer was lost, however, beyond  $R_t$  in the lower resolution model (33% as compared to 47%). Such a difference would be expected if the lower resolution allowed more cooling in the supernova-heated gas, reducing its buoyancy.

In Model C3, cooling was allowed at shock fronts, but was still prevented during the initial expansion of the hot gas. As compared to Model C1, Model C3 lost noticeably less tracer and mass beyond  $R_t$ , with at least 25% reductions relative to Model C1. These results confirm our suspicion that allowing cooling in the under-resolved shock fronts results in a noticeable increase in radiative losses, though the effect upon the evolution is not overly large.

The results of Model C4, in contrast, suggest that the technique of turning off the cooling in the initial

supernova region until it doubles in radius has only a small effect upon the final results. This result implies that the gas radiates away relatively little energy before the Sedov-Taylor solution is reached.

In Model C5, radiative cooling is allowed everywhere and at all times. As would be expected from the above results, the results of Model C5 are very similar to those of Model C3.

Model C6 is similar to Model C1, except that we assume a metallicity for the gas of  $Z = 0.3Z_{\odot}$ , ten times larger than that of Model C1. As can be seen in the table, this has no noticeable impact upon the results. From this, we conclude that, by the time the post-shock gas temperature drops to below  $10^4$  K, where metal cooling dominates, the evolution of the gas is determined by the momentum given to it by the shock, and is no longer affected by shock-heating.

In Model C7, we examine the effects of turning off radiative cooling completely, i.e. the gas evolves adiabatically from its initial conditions. As would be expected from earlier work (Larson 1974), the differences with all of the other models are dramatic. In Model C7, most of the original gas in the galaxy ( $\approx 80\%$ ) is expelled due to the energy input of the 10 supernovae, consistent with the estimate of the binding energy of galaxy Model 1. Similarly, almost all of the tracer material is lost.

From these results, we conclude, consistent with earlier studies, that radiative losses are crucial to the ability of dwarf galaxies to retain gas following supernova explosions. Numerical techniques employed to improve the accuracy of simulations, by turning off cooling in regions where overcooling is likely to occur, have quantitative effects upon the results, but do not affect qualitative conclusions that significant amounts of both tracer and gas are lost to the systems. The metallicity of the gas is found not to be a significant factor.

### 3.3. Multiple Supernovae in Systems with an Irregular ISM

Models G and H use, respectively, the low- and high- mass galaxy models. As in Models C and E, 10 supernovae are triggered over a timescale of 10 Myr. They differ from those earlier models in containing 100 low-density bubbles, which are intended to simulate an irregular ISM, as described in § 2.7. In Figure 7 are shown snapshots of density evolution in the central galactic plane for Model G, covering the same time span as those in Figure 2. The frothy nature of the initial gas distribution is clearly illustrated in the first few frames. As described in § 2, the bubbles are allowed to cool after  $\tau_{SN} + 0.5\tau_d$  (34.1 Myr for galaxy Model 1 and 75 Myr for galaxy Model 2). The cooling evolution is apparent in the eleventh frame of Figure 7. In Figure 8 is shown the evolution of the same tracer fluid as in Figure 3, now for Model G.

The evolution of the tracer and the mass for the two models are shown in Figures 9 and 10. The reduction of the average density in the cores of the models, and the presence of low density channels lead to dramatic differences from the earlier models. Nearly all of the enriched material is lost from the cores of both models. Approximately 70% is lost beyond  $R_t$  as well for Model G, while approximately 50% is lost beyond  $R_t$  for Model H. The systems also show mass losses of 40-50%.

As in Model C, the loss of tracer from the cores of Models G and H is accompanied by mass loss. Unlike the tracer loss, the mass loss later reverses, again implying poor mixing of the enriched gas within the galactic cores. Unlike the earlier model, the core masses eventually overshoot their initial values. The overshoot is due to the cooling of the bubbles, which causes some inflow into the central regions. As before, the enriched material which is lost beyond  $R_t$  is poorly mixed, as can be seen in Figure 8.

#### 4. Differences Between the Models

Models which included only a single supernova generally showed little loss of tracer material. In the case of supernovae centered in the galaxies, no tracer was lost even from the core of the galaxy. In the case of off-center supernovae, only the low mass system lost some of the enriched gas beyond the tidal radius. Such a lack of any effect may be surprising, given the weak gravitational binding energy of the gas,  $\Phi$ , in the two model galaxies, as shown in Table 1. In Model 1, for example,  $\Phi = 9.8 \times 10^{50}$  ergs, comparable to the energy of a single supernova. As discussed below, however, the relatively high gas densities of the systems allow them to radiate away the deposited energy relatively efficiently, with the result that a single supernova has little overall effect upon the systems.

The occurrence of multiple supernovae enhances the loss of enriched material in a few different ways. Early supernovae disturb the gas in the core of the galaxies, reducing the average density. The cooling efficiency of the gas is therefore reduced, as is the mass of gas available to physically contain the ejecta from later events. Later events may also help to give a “boost” to the enriched material from earlier events, as can be seen in Figure 3, being especially apparent at the times 3.8 and 7.7 Myr. Note that the apparent acceleration in the evolution of the tracer between 24.1 and 33.7 Myr is an illusion caused by the increasing time interval between frames.

The differences among the models with multiple supernovae are due to their different masses, and their relative abilities to cool within a dynamical timescale. As shown in Table 1, Models 1 and 2 have very similar central densities. Their different core radii therefore lead directly to different core masses, as discussed in § 3.1, with Model 2 having a greater amount of mass available to contain supernova ejecta than Model 1.

In the absence of cooling, the hot, enriched material from the supernovae would still eventually leave the galaxies due to their buoyancy. Radiative cooling prevents this, and the different size scales for the two galaxy models lead to very different ratios of cooling to dynamical times. The dynamical timescales from Equation (3-1) are  $\tau_d = 47$  and 128 Myr for galaxy Models 1 and 2, respectively. The cooling timescale is defined as (Field 1965)

$$\tau_c \sim \frac{\frac{3}{2}k_B T}{n_H L(T, Z)}, \quad (4-1)$$

where  $L = \Lambda/n_H^2$  is the cooling efficiency in  $\text{erg cm}^3 \text{s}^{-1}$ , and  $n_H$  is the number density of hydrogen. Close to their initial temperatures, and using our assumed metallicities,  $\tau_c \approx 36$  and 39 Myr, for Models 1 and 2 respectively. The initial cooling of the supernova-heated gas shall be much more efficient, with a correspondingly shorter timescale. For the gas to cool to its initial temperature, however, shall require timescales on the order of those calculated above. For Models 1 and 2, we find, respectively,  $\tau_c/\tau_d = 0.77$  and 0.30. The values for  $\tau_d$  would be smaller, and the timescale ratios larger by a factor of three had we used  $R_c$  instead of  $R_t$  in Equation (3-1).

The higher mass galaxy model is therefore able to cool much more on a dynamical timescale than is the lower mass model. Following the conversion of the deposited energy into kinetic energy, the high mass model can thus radiate away much of the energy before the enriched material can evolve significantly in space, further enhancing the ability of the more massive system to retain the enriched gas. This result is consistent with the observed correlation between metallicity and total mass in dSph’s (Mateo 1998).

The above factors work together to explain the differences seen between the pair of Models C1 and D, which use the low-mass galaxy model, and the pair of Models E and F, which use the high-mass galaxy model. In the first pair, almost all of the enriched gas is lost from within  $R_c$ , and both lose a significant

amount beyond  $R_t$ . Both models also show a substantial amount of mass loss. In Models E and F, however, less enriched material is lost from within  $R_c$ , almost none is lost from  $R_t$ , and there is much less mass loss.

The ability of the galaxy to cool between supernova events can also explain the differences between Models C1 and D, seen in Figure 4. In Model C1, the supernovae occur over a total time of 10 Myr, and the galaxy is unable to cool significantly between events, whereas the longer 100 Myr supernova timescale of Model D allows the system to radiate a significant amount of energy between supernovae. As compared to Model D, then, the supernovae have a much stronger cumulative effect in Model C1, leading to more rapid loss of enriched material from the core, as well as loss beyond  $R_t$ . The implication of these models is that star-burst events do not necessarily lead to greater enrichment of residual gas than does continuous star formation.

The differences between Models E and F are less striking than those between C1 and D, due primarily to the fact that the more massive system is able to retain enriched material as a whole more efficiently than the less massive system. As can be seen in Figure 6, there is less loss from the core of enriched material from a few of the supernovae in Model F as compared to Model E, which primarily accounts for the quantitative differences between the two models. Those supernovae happened to occur at late times, as the system was “recovering” from the earlier supernova events.

Models G and H were identical, respectively, to Models C1 and E, except for the presence of bubbles. The large filling factors of the bubbles in the models dramatically altered the evolution of the tracer. The bubbles reduce the amount of mass in the core of the galaxy, and increase the average cooling time of the galaxy. They also provide many channels for enriched gas to exit the core. As a result, most of the tracer is lost beyond  $R_c$  in both models, and a significant fraction is lost beyond  $R_t$ . Both models also lose 40-50% of the ambient gas. This result can be used to infer an upper limit on the rate of massive star production in order for there to be sufficient retained gas to fuel subsequent generations of star formation.

## 5. Consequences for the Evolution of Dwarf Spheroidal Galaxies

We have performed three-dimensional, numerical simulations of the evolution of enriched material from supernovae in dwarf spheroidal galaxies. The simulations have included either one or ten supernovae, and in the case of multiple supernovae, they have occurred over timescales of either 10 or 100 Myr. Two different galaxy models, 1 and 2, have been considered, chosen to approximate the parameters for the Leo II and Fornax dSph’s, respectively. Within these galaxy models, both smooth and irregular ISM distributions have been considered. The results of the models, discussed in § 3 and 4, are summarized in Table 3. We now discuss the possible consequences of our results for the evolution of dSph’s.

Our results indicate that, for extremely low star formation efficiencies, such as would lead to individual supernovae widely separated in time, it is difficult to expel enriched material completely from dwarf spheroidal galaxies (dSph’s) having an undisturbed ISM. In lower-mass systems, however, most enriched gas is lost from the cores of the galaxies following multiple supernovae, and a significant fraction is lost to the galaxy as a whole. In a system that has undergone a recent burst of star formation, however, the ISM is likely to be highly disturbed. We find that the presence of an irregular ISM greatly enhances the loss of enriched material both from the core as well as from the galaxy as a whole, in both low and high mass models. In all cases, the material is lost quickly, leaving the core within  $0.2\tau_d$  after the supernovae. Enriched material that is lost to the galaxy is typically lost within  $2\tau_d$ . As can be seen in the tracer plots, enriched gas does not mix well prior to being lost to the galaxy, leading to highly enriched “blobs” of material escaping beyond  $R_t$ .

The preferential loss of enriched gas from the cores of dSph’s might potentially lead to an “inverse” metallicity gradient, the consequences of which for subsequent star formation depend upon where later generations of stars form. If subsequent star formation is triggered by relatively quiescent processes, such as tidal compression, or runaway cooling resulting from self-shielding from external radiation, then star formation is expected to occur primarily in regions where the gas density is highest, i.e. in the core. In such cases, star formation shall occur in gas which is not heavily enriched from the previous generation of stars, with the result that multiple generations of stars could be present in the galaxy without strong metallicity variations. Given that the ISM is likely to be highly disturbed by the presence of hot stars, our models indicate that, in this case, poor self-enrichment efficiency is likely to be the norm in dSph’s.

Star formation triggered by localized compressions may, in contrast, occur at larger radii, where the gas may have been previously enriched. This might occur, for example, due to collisions between dwarf systems, encounters with a jet from a nearby massive galaxy, or due to the infall of material onto the dwarf galaxy. The latter case might well be the result of infall of material that was originally expelled from the dwarf itself. When material in our simulations is lost from the galaxies, it exits at below the sound speed ( $\lesssim 10 \text{ km s}^{-1}$ ), much less than the orbital speed of dwarf galaxies around systems such as the Milky Way. The ejected gas shall, therefore, follow a similar orbit around the parent galaxy, and may collide with gas remaining within the dwarf system due to orbit crossing at apogalacticon (Dong, Lin, & Oh 2002). Such an encounter might lead to star formation at large radii in the dwarf, and a subsequent generation of stars showing significant metallicity enhancement.

Enriched gas which accumulates in the outer regions of dwarf galaxies may eventually be lost to the galaxy through ram-pressure stripping, tidal effects, or due to subsequent generations of star formation in the core. Thus, as much as 90% of the supernova ejecta could be lost, and may enrich the halo of a nearby massive galaxy. The halo of the Milky Way, for example, could have been enriched to its average metallicity by a population of dwarf spheroidals ten times larger than the number currently observed.

This work was performed under the auspices of the U.S. Department of Energy by University of California, Lawrence Livermore National Laboratory under Contract W-7405-Eng-48. This work is partially supported by NASA through an astrophysical theory grant NAG5-12151.

## REFERENCES

- Andersen, R.-P., & Burkert, A. 2000, *ApJ*, 531, 296
- Anninos, P., & Fragile, P. C. 2003, *ApJS*, 144, 243
- Anninos, P., Fragile, P. C., & Murray, S. D. 2002, *ApJ*, submitted
- Anninos, W. Y., & Norman, M. L. 1994, *ApJ*, 429, 434
- Babul, A. & Rees, M. J. 1992, *MNRAS*, 255, 346
- Barkana, R., & Loeb, A. 1999, *ApJ*, 523, 54
- Benson, A. J., Lacey, C. E., Baugh, C. M., Cole, S., & Frenk, C. S. 2002, *MNRAS*, 333, 156
- Binney, J. & Tremaine, S. 1987, *Galactic Dynamics* (Princeton: Princeton Univ. Press)
- Blondin, J. M., Fryxell, B. A., & Konigl, A. 1990, *ApJ*, 360, 370
- Blumenthal, G. R., Faber, S. M., Primack, J. R., & Rees, M. J. 1984, *Nature*, 311, 517
- Burkert, A. 2000, *ApJ*, 534, L143
- Burkert, A. 1995, *ApJ*, 447, L25
- Cole, S., Aragon-Salamanca, A., Frenk, C. S., Navarro, J. F., & Zepf, S. E. 1994, *MNRAS*, 271, 781
- Côté, P., Oke, J. B., & Cohen, J. G. 2000, *AJ*, 118, 1645
- Dekel, A., & Silk, J. 1986, *ApJ*, 303, 39
- Dohm-Palmer, R. C., Skillman, E. D., Gallagher, J. S., Tolstoy, E., Mateo, M., Dufour, R. J., Saha, A., Hoessel, J., & Chiosi, C. 1998, *AJ*, 116, 1227
- Dohm-Palmer, R. C., Skillman, E. D., Mateo, M., Saha, A., Dolphin, A., Tolstoy, E., Gallagher, J. S. & Cole, A. A. 2002, *AJ*, 123, 813
- Dohm-Palmer, R. C., Skillman, E. D., Saha, A., Tolstoy, E., Mateo, M., Gallagher, J. S., Hoessel, J., Chiosi, C., & Dufour, R. J. 1998, *AJ*, 114, 2527
- Dong, S., Lin, D. N. C., & Oh, K. S. 2002, in preparation
- Dong, S., Murray, S. D., & Lin, D., N. C. 2002, *ApJ*, submitted
- Efstathiou, G. 1992, *MNRAS*, 256, 43P
- Field, G. B. 1965, *ApJ*, 142, 531
- Gallagher, J. S., Tolstoy, E., Dohm-Palmer, R. C., Skillman, E. D., Cole, A. A., Hoessel, J. G., Saha, A., & Mateo, M. 1998, *AJ*, 115, 1869
- Grebel, E. K. 2001, *ASSS*, 277, 231
- Grebel, E. K. 1997, *Rev. Mod. Astron.*, 10, 29

- Harbeck, D., Grebel, E. K., Holtzmann, J., Guhathakurta, P., Brandner, W., Geisler, D., Sarajedini, A., Dolphin, A., Hurley-Keller, D., & Mateo, M. 2001, *AJ*, 122, 3092
- Heiles, C. 1987, *Interstellar Processes*, ed. D. J. Hollenbach & H. A. Thronson, (Dordrecht: D. Reidel), 171
- Kepner, J. V., Babul, A., & Spergel, D. N. 1997, *ApJ*, 487, 61
- Klypin, A., Kravtsov, A. V., Valenzuela, O., & Prada, F. 1999, *ApJ*, 522, 82
- Klypin, A., Nolthenius, R., & Primack, J. 1997, *ApJ*, 474, 533
- Larson, R. B. 1974, *MNRAS*, 169, 229
- Lehnert, M. D., Bell, R. A., Hesser, J. E., & Oke, J. B. 1992, *ApJ*, 395, 466
- Lin, D. N. C., & Murray, S. D. 1994, *Dwarf Galaxies* (Garching: ESO), 535
- Mac Low, M.-M., & Ferrara, A. 1999, *ApJ*, 513, 142
- Mac Low, M.-M., & McCray, R. 1988, *ApJ*, 324, 776
- Madau, P., Ferrara, A., & Rees, M. J. 2001, *ApJ*, 555, 92
- Mateo, M. 1998, *ARA&A*, 36, 435
- Mori, M., & Burkert, A. 2000, *ApJ*, 538, 559
- Mori, M., Ferrara, A., & Madau, P. 2002, *ApJ*, 571, 40
- Mori, M., Yoshii, Y., Tsujimoto, T., & Nomoto, K. 1997, *ApJ*, 478, L21
- Murray, S. D., Dong, S., & Lin, D. N. C. 2003, *ApJ*, submitted
- Navarro, J. F., Frenk, C. S., & White, S. D. M. 1997, *ApJ*, 490, 493
- Navarro, J. F., & Steinmetz, M. 1997, *ApJ*, 478, 13
- Navarro, J. F., & White, S. D. M. 1994, *MNRAS*, 267, 401
- Noriega-Crespo, A., Bodenheimer, P., Lin, D. N. C., & Tenorio-Tagle, G. 1989, *MNRAS*, 237, 46
- Peebles, P. J. E., & Dicke, R. H. 1968, *ApJ*, 154, 891
- Persic, M., Salucci, P., & Stel, F. 1996, *MNRAS*, 281, 27
- Quinn, T., Katz, N., & Efstathiou, G. 1996, *MNRAS*, 278, L49
- Rosner, R. & Tucker, W. H. 1989, *ApJ*, 338, 761
- Shapiro, P. R., & Struck-Marcell, C. 1985, *ApJS*, 57, 205
- Shetrone, M. D., Côté, P., & Sargent, W. L. W. 2001, *ApJ*, 548, 592
- Smecker-Hane, T. A., Stetson, P. B., Hesser, J. E., & Vandenberg, D. A. 1996, in *From Stars to Galaxies: The Impact of Stellar Physics on Galaxy Evolution*, ed. C. Leitherer, U. Fritze-von Alvensleben, & J. Huchra (San Francisco: ASP), 328

Sommer-Larsen, J., Gelato, S., & Vedel, H 1999, *ApJ*, 519, 501

Spitzer, L. 1956, *Physics of Fully Ionized Gases* (New York: Interscience)

Suntzeff, N. B., Mateo, M., Terndrup, D. M., Olszewski, E. W., Geisler, D., & Weller, W. 1993, *ApJ*, 418, 208

Tenorio-Tagle, G., Bodenheimer, P., Lin, D. N. C., & Noriega-Crespo, A. 1986, *MNRAS*, 221, 635

Weil, M. L., Eke, V. R., & Efstathiou, G. 1998, *MNRAS*, 300, 773

Weinberg, D. H., Hernquist, L., & Katz, N. 1997, *ApJ*, 477, 8

White, S. D. M., & Rees, M. J. 1978, *MNRAS*, 183, 341



Table 1. Galaxy Parameters

| Galaxy | $M_d$<br>( $10^6 M_\odot$ ) | $M_g$<br>( $10^6 M_\odot$ ) | $R_c$<br>(pc) | $\rho_0$<br>( $10^{-24} \text{ g cm}^{-3}$ ) | $\tau_d$<br>(Myr) | $\Phi$<br>( $10^{51} \text{ erg}$ ) | $E_{th}$<br>( $10^{51} \text{ erg}$ ) |
|--------|-----------------------------|-----------------------------|---------------|--|-------------------|-------------------------------------|---------------------------------------|
| 1      | 10                          | 1.0                         | 130           | 1.2  | 47                | 0.98                                | 2.5                                   |
| 2      | 55                          | 5.5                         | 360           | 1.1  | 128               | 16.                                 | 12.                                   |

Table 2. Model Parameters

| Model | Galaxy | $N_{SN}$ | $\tau_{SN}$<br>(Myr) | $N_{\text{bub}}$ |
|-------|--------|----------|----------------------|------------------|
| A     | 1      | 1        | –                    | 0                |
| B     | 2      | 1        | –                    | 0                |
| C     | 1      | 10       | 10                   | 0                |
| D     | 1      | 10       | 100                  | 0                |
| E     | 2      | 10       | 10                   | 0                |
| F     | 2      | 10       | 100                  | 0                |
| G     | 1      | 10       | 10                   | 100              |
| H     | 2      | 10       | 10                   | 100              |

Table 3. Results of the Models

| Model | Core tracer loss<br>% | Total tracer loss<br>% | Mass loss<br>% |
|-------|-----------------------|------------------------|----------------|
| A1    | 0                     | 0                      | 10             |
| A2    | 92                    | 30                     | 7              |
| B1    | 0                     | 0                      | 3              |
| B2    | 98                    | 0                      | 2              |
| C1    | 94                    | 47                     | 36             |
| C2    | 93                    | 33                     | 33             |
| C3    | 90                    | 30                     | 27             |
| C4    | 94                    | 50                     | 35             |
| C5    | 91                    | 29                     | 26             |
| C6    | 94                    | 47                     | 36             |
| C7    | 100                   | 84                     | 80             |
| D     | 79                    | 19                     | 21             |
| E     | 65                    | 3                      | 10             |
| F     | 59                    | 0                      | 7              |
| G     | 99                    | 71                     | 51             |
| H     | 94                    | 46                     | 37             |

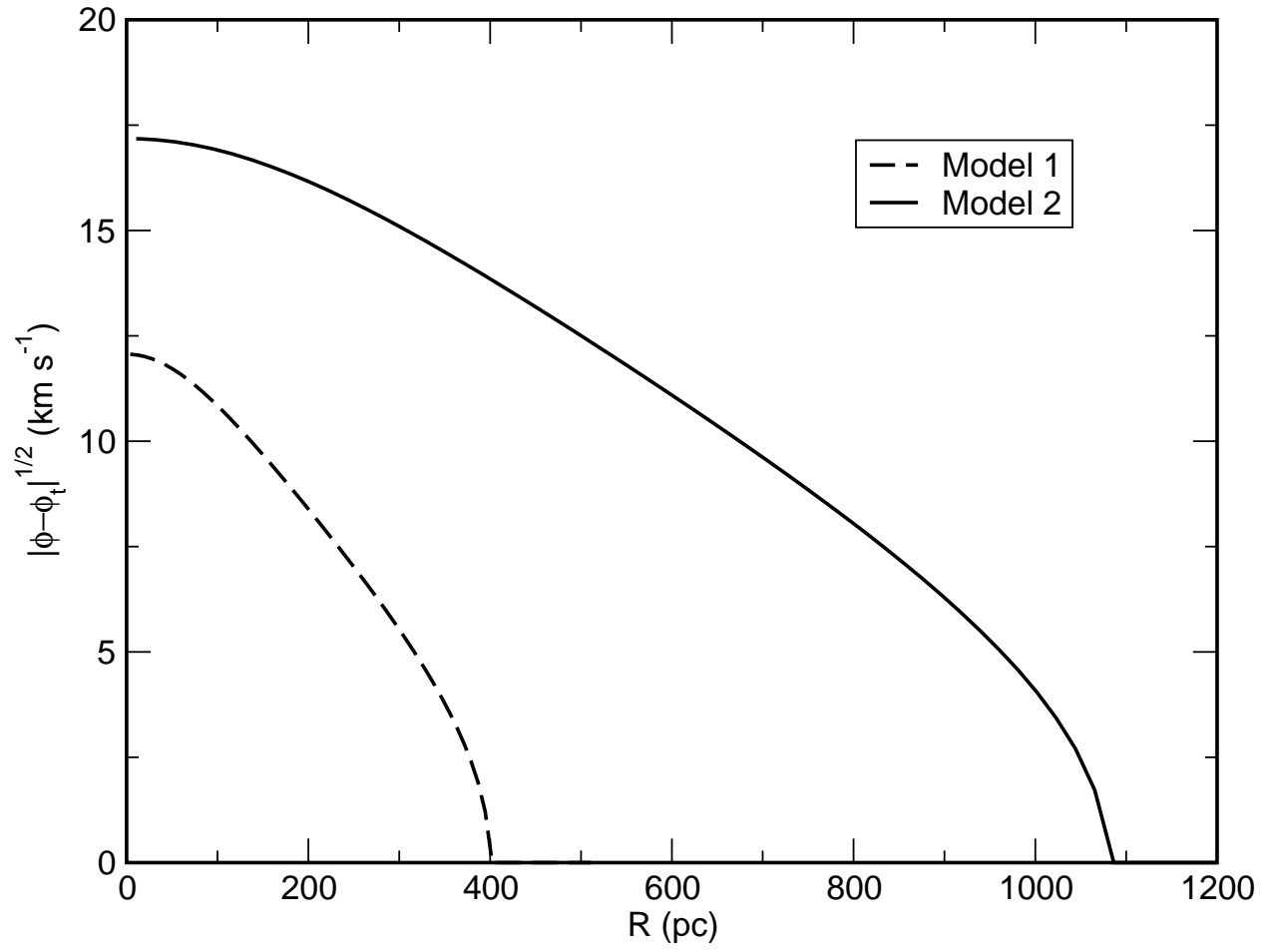


Fig. 1.— Square root of the absolute value of the normalized gravitational potential as a function of radius for galaxy model 1 (dashed curve) and galaxy model 2 (solid curve).

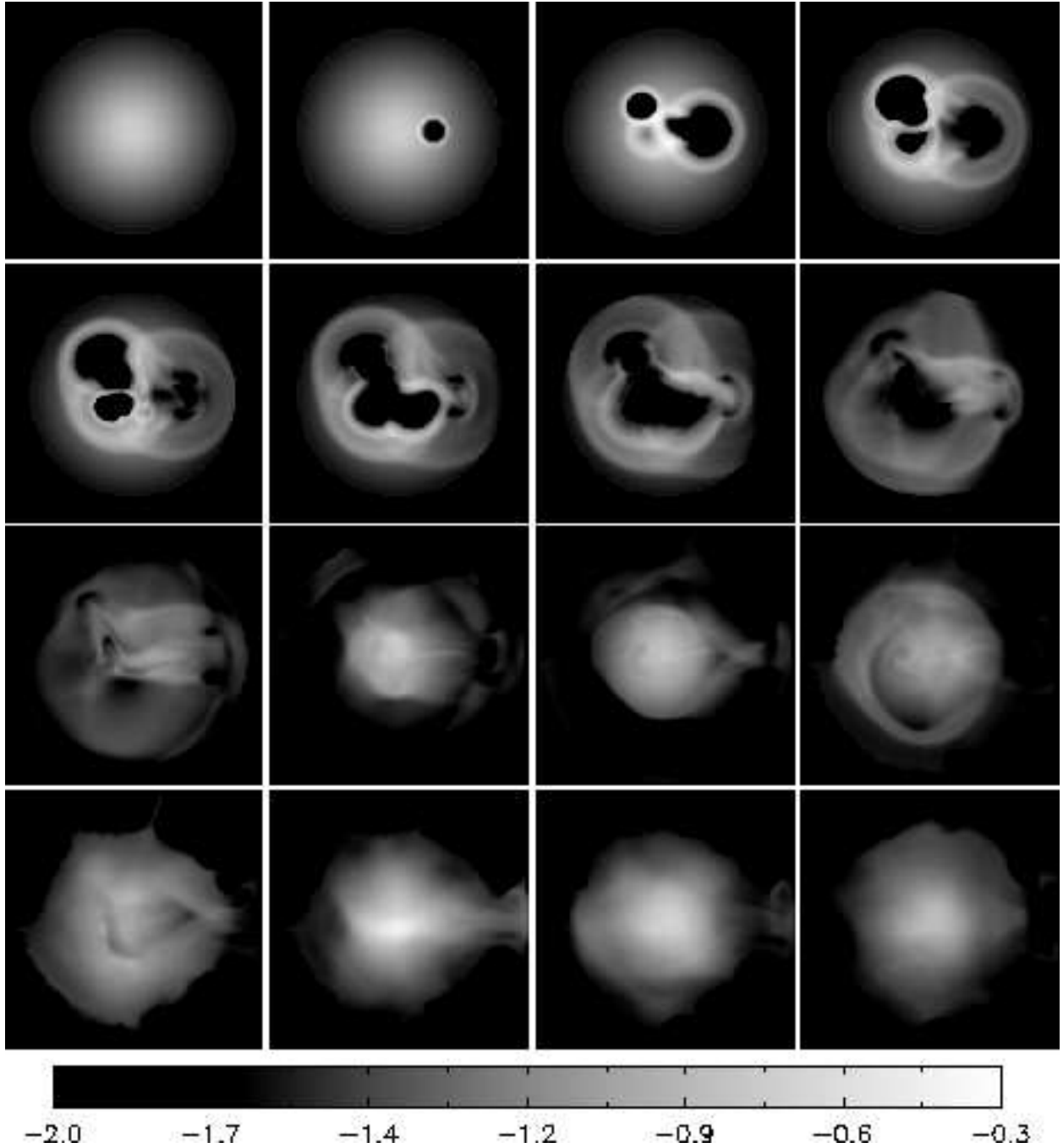


Fig. 2.— Slices through the central plane of the galaxy showing the evolution of the logarithm of gas density for Model C1 at times 0, 0.24, 3.8, 7.7, 9.6, 12.1, 14.5, 19.3, 24.1, 33.7, 43.4, 53.0, 62.7, 72.3, 81.9, and 96.4 Myr. The units for the density scale in this plot are  $5.9 \times 10^{-24} \text{ g cm}^{-3}$ .

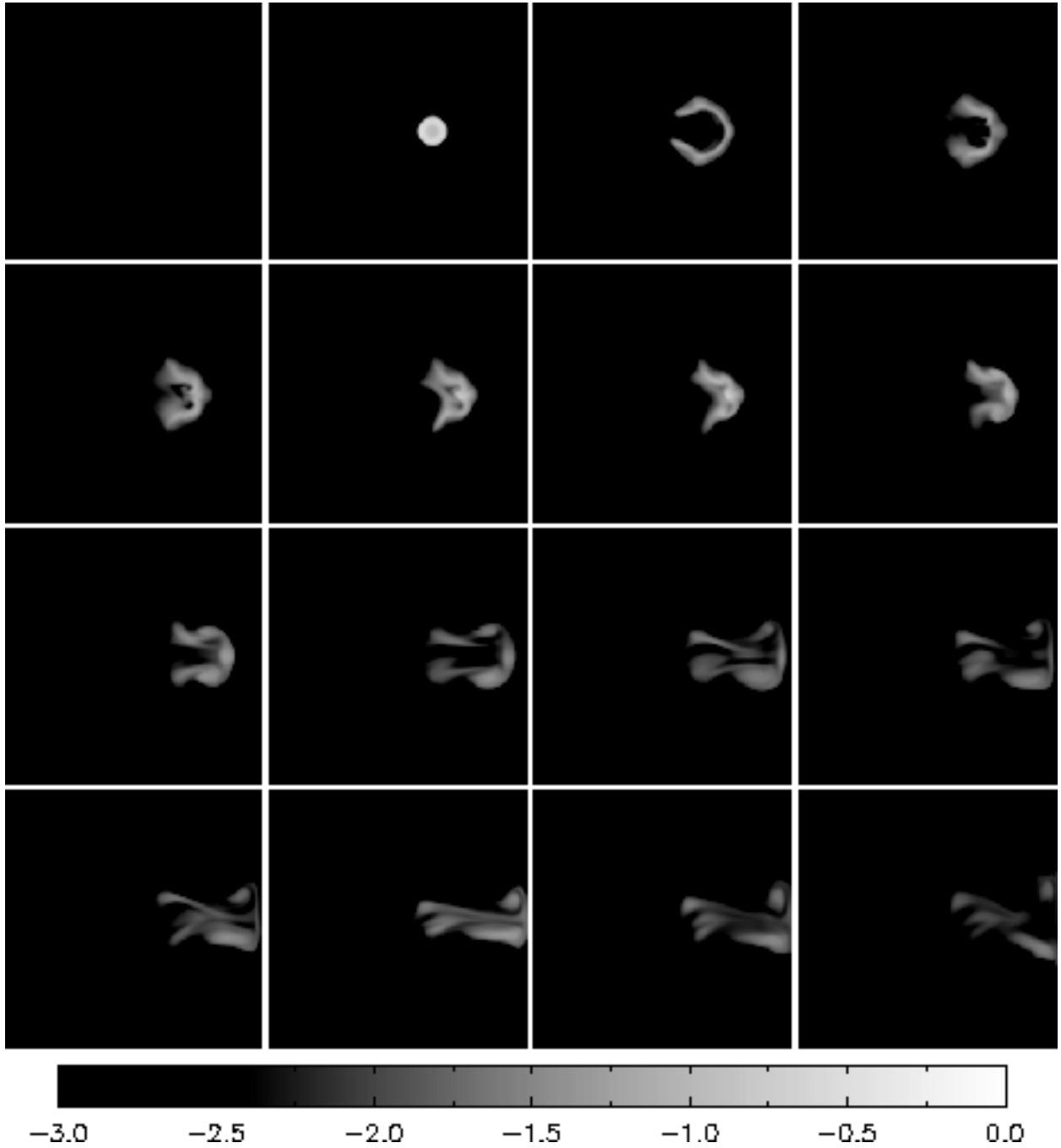


Fig. 3.— Slices through the central plane of the galaxy showing the evolution of a single tracer fluid for Model C1. The frames correspond to those shown in Figure 2. The tracer fluid belongs to the first supernova (triggered at  $R_c$ ), visible in the second frame of Figure 2. The logarithmic scale shows the relative amount of tracer found in different regions.

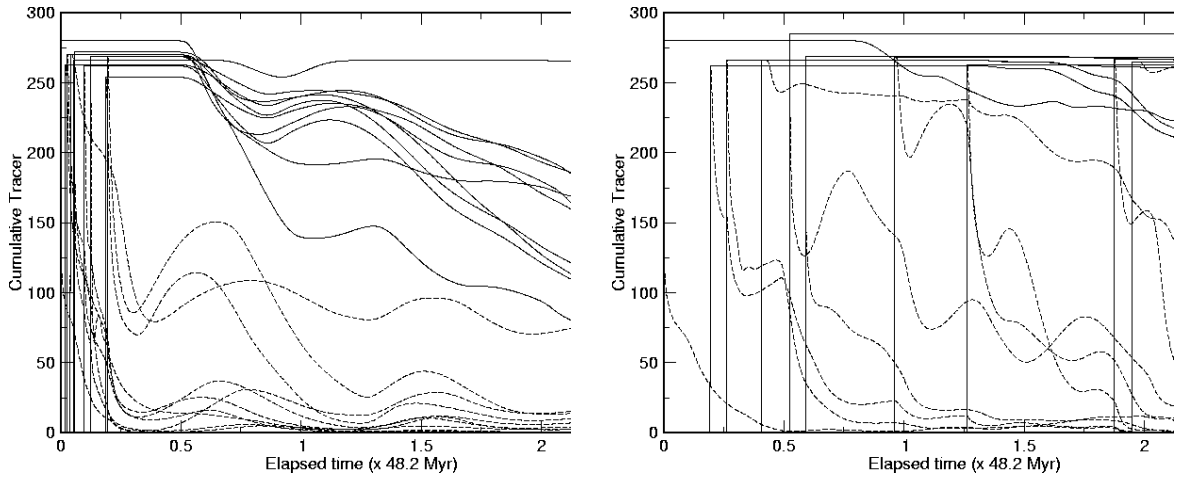


Fig. 4.— Tracer evolution for (a) Model C1 and (b) Model D. Shown are the amount of tracer for each supernova contained within the tidal radius (solid curves) and within the core radius (dashed curves) as a function of the elapsed time.

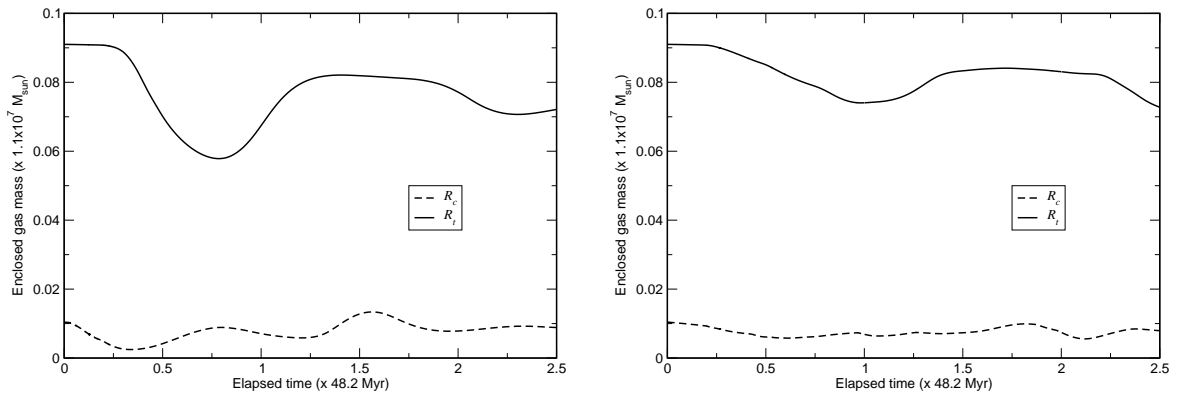


Fig. 5.— Mass evolution of (a) Model C1 and (b) Model D. Shown for each model is the gas mass within the tidal radius  $R_t$  (solid curves) and the core radius  $R_c$  (dashed curves) as a function of time.



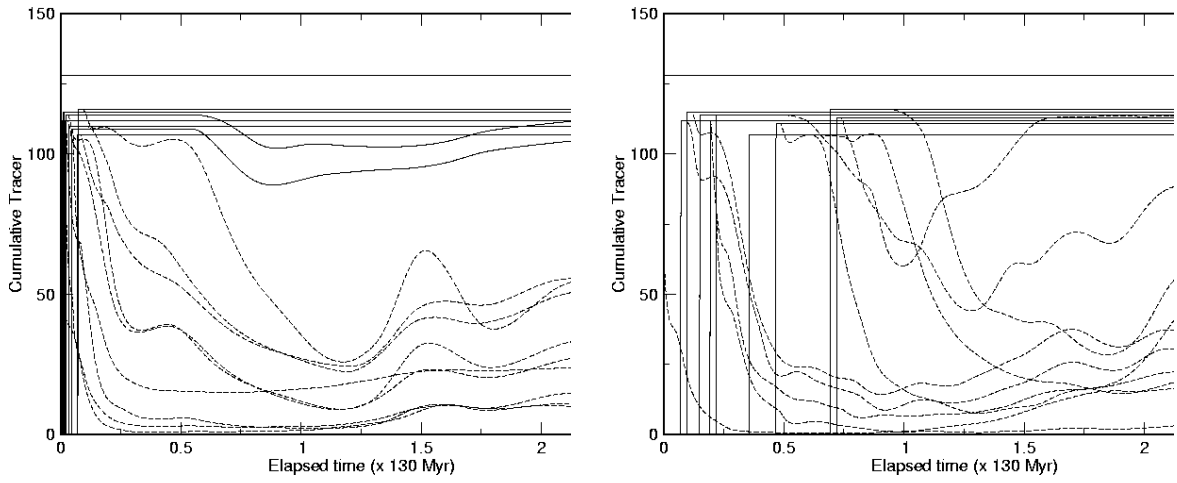


Fig. 6.— As Figure 4, but for (a) Model E and (b) Model F. The results are displayed as in Figure 4.

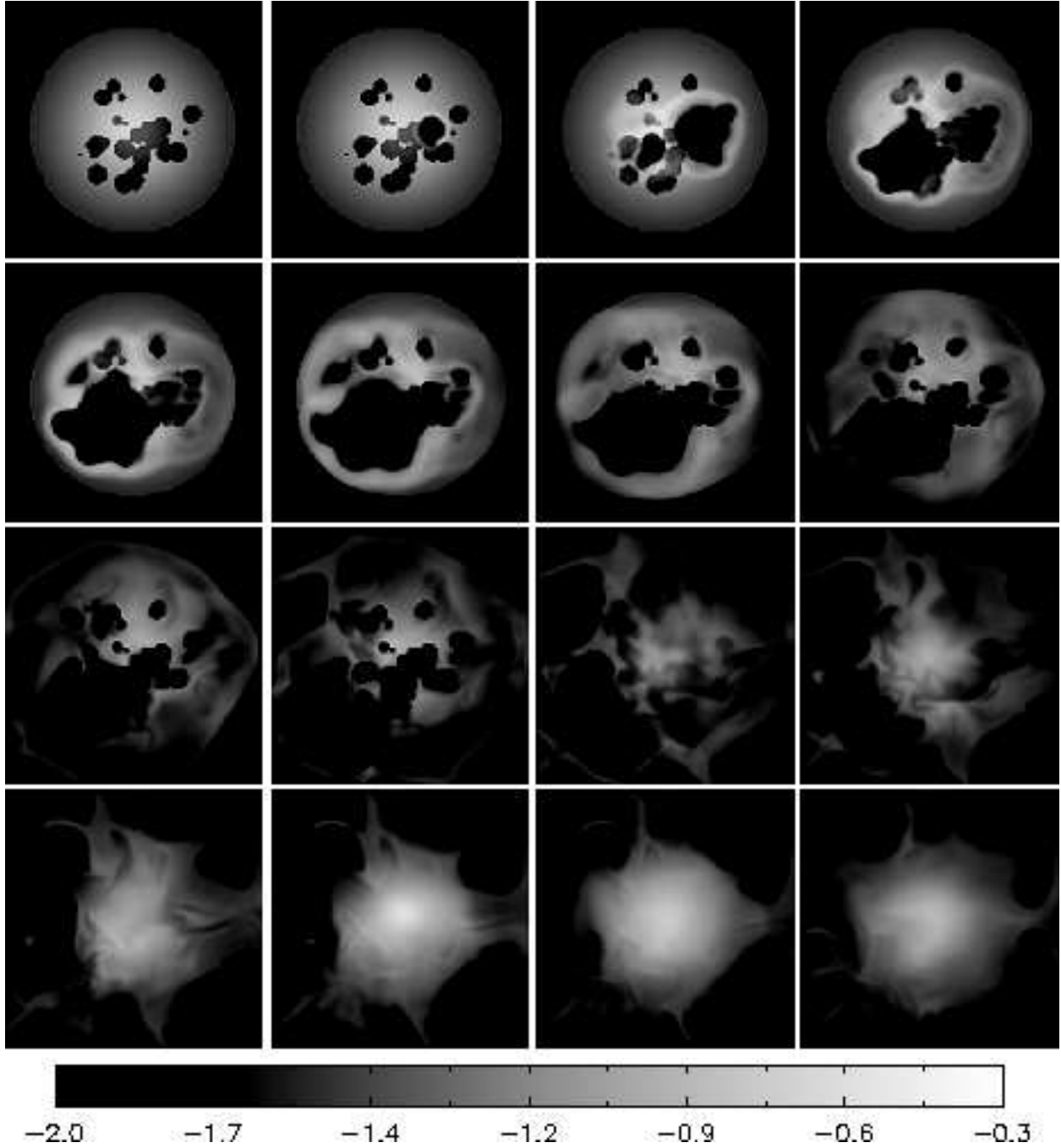


Fig. 7.— Slices through the central plane of the galaxy showing the evolution of the logarithm of gas density for Model G. The frames correspond to those shown in Figure 2.

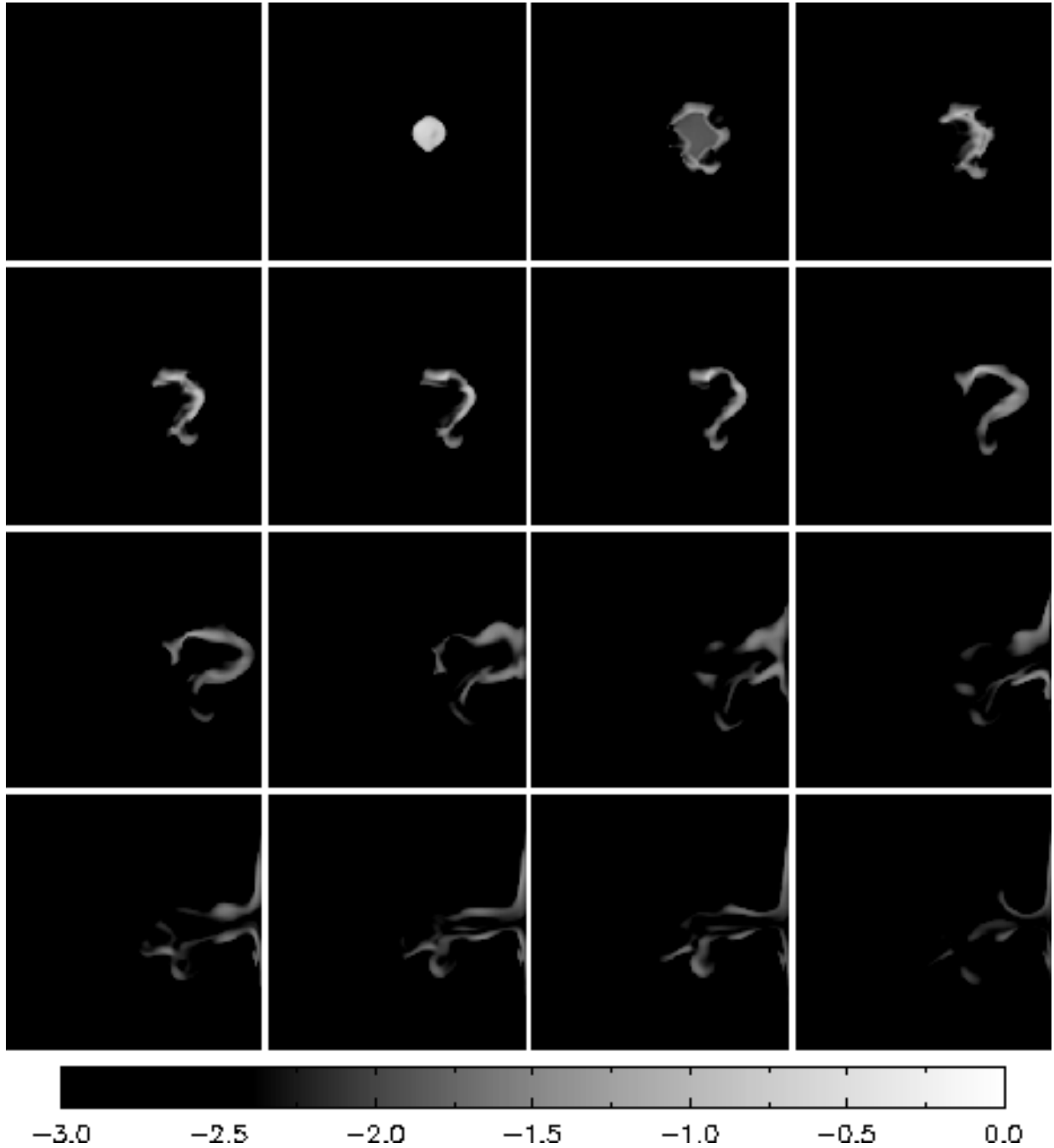


Fig. 8.— Slices through the central plane of the galaxy showing the evolution of a single tracer fluid for Model G. The frames correspond to those shown in Figure 2. Again the tracer fluid belongs to the first supernova, visible in the second frame of Figure 7.

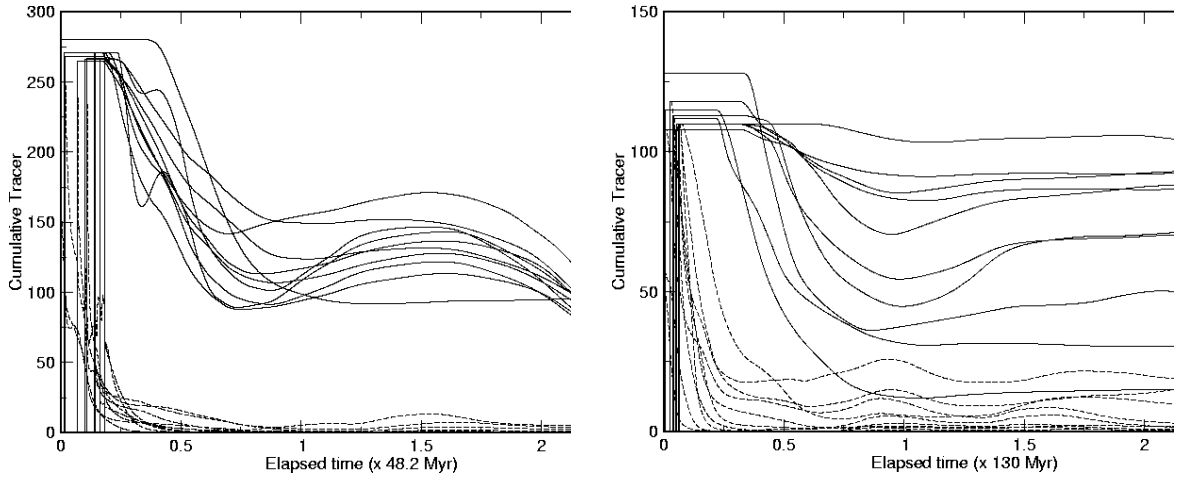


Fig. 9.— As Figure 4, but for Models G and H.

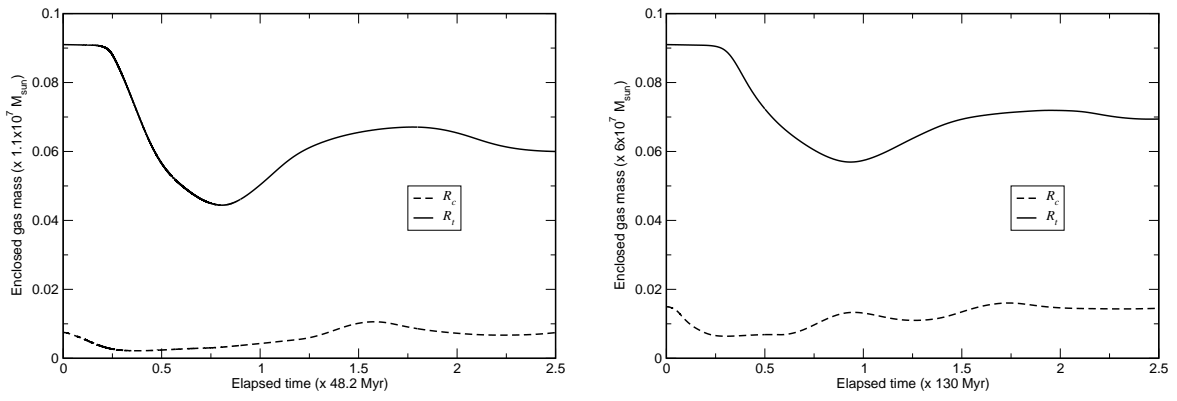


Fig. 10.— As Figure 5, but for Models G and H.